# SiD Letter of Intent

October 2008

Editors: H. Aihara, P. Burrows, M. Oreglia

# Contents

0.1 Forward Detector . . . . . . . . . . 2

0.2 Design criteria . . . . . . . . . . 2

0.2.1 LumiCal Physics Requirements . . . . . . . . . . 2

0.2.2 Luminosity precision and detector alignment . . . . . . . . . . 3

0.2.3 Monitoring the Instantaneous Luminosity with BeamCal . . . . . . . . . . 3

0.2.4 Detector Hermeticity . . . . . . . . . . 4

0.2.5 Dynamic range and mip sensitivity . . . . . . . . . . 4

0.2.6 Radiation hardness . . . . . . . . . . 4

0.2.7 Occupancy . . . . . . . . . . 5

0.3 Baseline Design . . . . . . . . . . 5

0.4 Expected Performance . . . . . . . . . . 7

0.4.1 Energy containment and energy resolution in LumiCal . . . . . . . . . . 7

0.4.2 Luminosity precision and LumiCal segmentation . . . . . . . . . . 8

0.4.3 Bhabha scattering . . . . . . . . . . 9

0.4.4 High energy electron detection in BeamCal . . . . . . . . . . 10

0.4.5 Calorimeter hermeticity . . . . . . . . . . 11

0.4.6 Tungsten mask . . . . . . . . . . 12

0.5 R&D . . . . . . . . . . 12

# List of Figures


1 Forward region. . . . . . . . . . . . . . . . . . . . . . . . . . . . . . . . . . . . . . 5

2 LumiCal sensor and segmentation. . . . . . . . . . . . . . . . . . . . . . . . . . . 7

3 BeamCal sensor and segmentation. . . . . . . . . . . . . . . . . . . . . . . . . . . 8

4 (a) Deposited energy in Si layers (b) Energy resolution . . . . . . . . . . . . . . 9

5 (a) Total energy distribution (b) Correlation of e+ and e- polar angles . . . . 10

6 Efficiency to reconstruct high energy electrons at three azimuthal angles . . . 11

7 Energy deposition in Si layers as a functon of $\cos\theta$ . . . . . . . . . . . . . . . . 12

8 Number of photons penetrating the tungsten mask as a function of the mask thickness 13

# List of Tables

1 LumiCal Parameters . . . . . . . . . . . . . . . . . . . . . . . . . . . . . . . . . 6
2 Radial segmentation . . . . . . . . . . . . . . . . . . . . . . . . . . . . . . . . . 9
3 Azimuthal segmentation . . . . . . . . . . . . . . . . . . . . . . . . . . . . . . . 10

## 0.1 Forward Detector

The forward region is defined as polar angles $|\cos\theta| > 0.99$ ($\theta < 140$mrad) forward of the SiD Endcap ECAL. The angular coverage is completed by two detectors, the Luminosity Calorimeter (LumiCal) and the Beam Calorimeter (BeamCal). The physics missions in this region are:

- precision measurement of the integrated luminosity using small-angle Bhabha scattering (LumiCal). To measure cross section of an event sample $O(10^6)$ expected for $e^+e^- \rightarrow W^+W^-$ in 5 years with 500 fb$^{-1}$, the goal is to measure the luminosity with an accuracy better than $10^{-3}$.
- precise determination of the luminosity spectrum by measuring the acolinearity angle of Bhabha scattering (LumiCal). Due to the beamstrahlung emission the colliding beams loose energies before collision, and the center-of-mass energy is no longer monochromatic. The luminosity spectrum affects mass measurement and threshold scan.
- extend the calorimeter hermeticity into the small angles for physics searches (LumiCal and BeamCal). An excellent hermeticity is essential as many new-physics reactions are accompanied with a large missing energy.
- instantaneous luminosity measurement using beamstrahlung pairs (BeamCal).
- two photon veto for new particle searches (BeamCal).

The detector challenges are good energy resolution, radiation hardness, interfacing with the final focus elements, high occupancy rate requiring special readout, and performing the physics measurements in the presence of the very high background in the forward direction.

## 0.2 Design criteria

### 0.2.1 LumiCal Physics Requirements

The lowest order Bhabha cross-section for $t$ channel one photon exchange is given by:

$$\frac{d\sigma}{d\Omega} = \frac{\alpha^2}{8E^2}\left(\frac{1+\cos^2\theta/2}{\sin^4\theta/2}\right)$$

We use this simple formula to estimate the polar angle coverage needed, although the complete electro-weak $s$ and $t$ channel cross-section will later be needed in order to do the physics. The number of Bhabha events per bunch crossing for a detector with minimum and maximum polar angle coverage $\theta_{min}$ and $\theta_{max}$ (in mrad) is:

$$N = 0.5\text{pb}\frac{\text{L}}{\text{R}}\int_{\theta_{\text{min}}}^{\theta_{\text{max}}}\frac{\text{dcos}\theta}{\sin^4\theta/2} \sim 8\left(\frac{1}{\theta^2_{\text{min}}} - \frac{1}{\theta^2_{\text{max}}}\right)$$

for $\sqrt{s}$=0.5 TeV, L=2×$10^{34}$cm$^{-2}$s$^{-1}$, and bunch crossing rate R=1.4 × $10^4$s$^{-1}$. Our goal is to measure the luminosity normalization with an accuracy of several $10^{-4}$ for $\sqrt{s}$=0.5 TeV. To do this one needs ≈ $10^8$ events collected over ≈ $10^7$ s, or about ten events per second. One can then calculate the absolute luminosity with ≈ 10% statistical error every several minutes during the run. With a bunch crossing rate of 1.4 × $10^4$s$^{-1}$, we need > $10^{-3}$ events per bunch crossing. To achieve this statistical accuracy, we start the fiducial region for the precision luminosity measurement well away from the beamstrahlung pair edge at $\theta_{min}$=20mrad, with a fiducial region beginning at 30mrad, which gives ≈ $10^{-2}$ events per bunch crossing.

### 0.2.2 Luminosity precision and detector alignment

The integrated luminosity, L is measured using the number of Bhabha events N and the Bhabha scattering cross section $\sigma$ in the detector fiducial region as $L = N/\sigma$. Since the Bhabha cross section is $\sigma \sim 1/\theta^3$, the luminosity precision can be expressed as

$$\frac{\Delta L}{L} = \frac{2\Delta\theta}{\theta_{min}},$$

where $\Delta\theta$ is a systematic error (bias) in polar angle measurement and $\theta_{min}$ is the minimum polar angle of the fiducial region. Because of the steep angular dependence, the precision of the minimum polar angle meaurement determines the luminosity precison. To reach the luminosity precision goal of $10^{-3}$, the polar angle must be measured with a precision $\Delta\theta <$ 0.02 mrad and the radial positions of the sensors must be controlled within 30 $\mu$m relative to the IP.

### 0.2.3 Monitoring the Instantaneous Luminosity with BeamCal

The colliding electron and positron bunches at the ILC experience intense electromagnetic fields as they pass each other. These fields generate large Lorentz forces, which cause radiation of gammas called beamstrahlung. A small fraction of the beamstrahlung gammas convert in pairs. Under the ILC Nominal beam parameters at $\sqrt{s} = 0.5$ TeV, approximately 75k $e^+/e^-$ are generated. The BeamCal intercepts ≈ 3 × $10^4$ beamstrahlung pairs of average energy ≈0.7 GeV per bunch crossing when the bunches have maximum overlap. Since the number of pairs is directly proportional to the beam overlap, the instantaneous luminosity can be monitored by detecting pairs in the BeamCal. Our goal is at the ten percent level per beam crossing.

The Detector Integrated Dipole (DID)[2] plays an important role in controlling the beamstrahlung pairs. The DID is a pair of coils wound on the detector solenoid, which creates sine-like transverse field. In the so-called Anti-DID configuration, the DID field effectively compensates the crossing angle for the outgoing beam and directs the low energy pairs into the extraction aperture, reducing the total pair energy hitting the BeamCal from 20 TeV to 10 TeV.

### 0.2.4 Detector Hermeticity

By hermeticity we mean an accurate measurement of the transverse momentum ($P_T$) balance in the event, which is achieved by good energy resolution, avoiding cracks, dead areas, and by covering down to small polar angles. The measurement of $e^+e^- \rightarrow slepton\ pairs$ in the presence of two photon background has been given as the performance detector design criteria for hermeticity[1]. In the stau production and decay,

$$e^+e^- \rightarrow \bar{\tau}\bar{\tau} \rightarrow \tau^+\chi^0\tau^-\chi^0$$

the $\chi^0$ is the LSP and escapes the detector. Under the SUSY dark matter scenario, the mass difference between stau and the LSP becomes less than 10 GeV, the missing $P_T$ is less and the measurements become more difficult. The main background comes from the two-photon process $e^+e^- \rightarrow e^+e^-X$, where X is $ee$, $\mu\mu$, or $\tau\tau$ for the slepton search. This background process has no missing $P_T$; however, if we miss both electrons then the missing $P_T < 2\theta_{min}E_{beam}$. This is the kinematic limit. Generally one photon is on-shell, so usually the missing $P_T < \theta_{min}E_{beam}$. The search region in the missing $P_T$ is determined by how small angle the two-photon electrons are detected and thereby vetoed. The electron detection must be made in the BeamCal where the beamstrahlung pairs deposit 10 TeV of energy.

### 0.2.5 Dynamic range and mip sensitivity

While minimum ionizing particles (MIP) deposit 93 keV in a 320 $\mu$m-thick Si layer, a 250 GeV electron can deposit up to 160 MeV or 1700 MIP equivalents in a single cell near shower maximum. If we want a 100% MIP sensitivity, the S/N ratio for MIP should be greater than 10, and the dynamic range of electronics need to be at least 17,000. This dynamic range can be achieved using 10 bits ADC with two gains.

### 0.2.6 Radiation hardness

The beamstrahlung pairs will hit the BeamCal, depositing 10 TeV of energy every bunch crossing. Sensor electronics could be damaged by the energy deposition, and sensor displacement damage could be caused by neutrons. The radiation dose varies significantly with radius, and a maximum dose of up to 100 MRad/year is expected at near the beampipe. The main source of neutrons is from secondary photons in the energy range 5-30 MeV, which excite the giant nuclear dipole resonance. The number of neutrons produced in one 0.5cm $\times$ 0.5cm BeamCal detector segment per year is approximately $5 \times 10^{13}$n/cm$^2$

### 0.2.7 Occupancy

The issue here is how "deep" we need to make the readout buffer to hold one train of events for the LumiCal. The LumiCal occupancy is studied for the beamstrahlung pairs and two-photon events. The occupancy from the pairs still dominates. In the far LumiCal just outside the pair edge, the number of hits will reach 120 hits per bunch train. The number of hits per bunch train decreases to four at approximately $R \sim 10$ cm in the near LumiCal.

## 0.3 Baseline Design

The layout of the forward region is illustrated in Figure 1. The LumiCal covers the polar angles from 40 mrad to 90 mrad, and the BeamCal from 3 mrad to 40 mrad. The conical mask made of 3cm-thick tungsten is located between the LumiCal and BeamCal. When the beamstrahlung pairs hit the BeamCal, low energy secondary particles are generated. The mask shields the SiD central detectors from low energy photons backscattered from the BeamCal. The Low-Z mask made of 13cm-thick Borated-Polyethylene is located in front of the BeamCal. The Low-Z mask reduces the low energy electron and positron albido from the BeamCal by more than an order of magnitude. Borated-Polyethylene also absorbs low energy neutrons produced in the BeamCal and directed toward the IP.

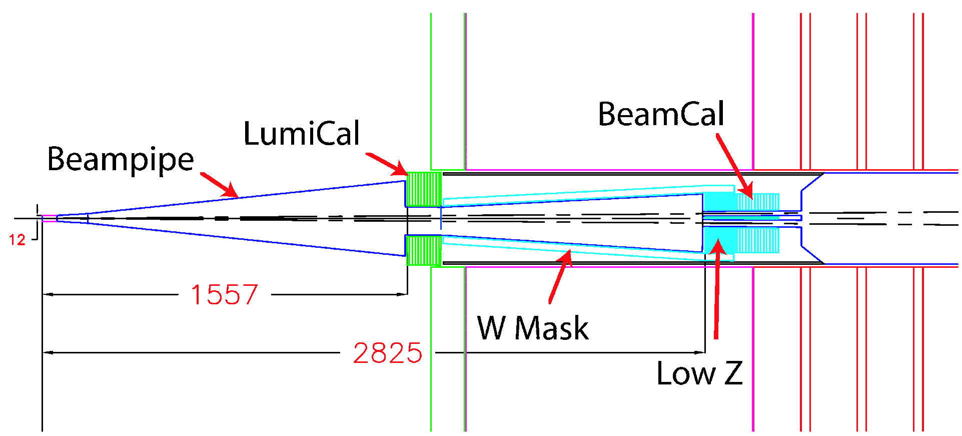


Figure 1: Forward region.

The beam pipe at the IP is made of beryllium to minimize multiple scattering. The inner radius is 1.2 cm, and the thickness is 400 $\mu m$. The conical section starts at R=1.2 cm, Z=6.25 cm, and flares to 103 mrad, which is outside of the LumiCal fiducial region. The flared beam pipe design allows particles to exit the beam pipe at normal incidence before entering the LumiCal. The cylindrical beam pipe inside the LumiCal is 6 cm in radius, and is centered on the extraction beam line to accommodate the 14 mrad crossing angle. The beam pipe does not intercept the beamstrahlung pairs which are confined within 4 cm radius by the SiD 5 Tesla solenoid.

The entire forward region is supported by the support tube which is cantilevered from the QD0 cryostat. There is a 1 cm gap between the support tube and the endcap door to facilitate the door opening. To minimize the electromagnetic energy loss due to the gap, the LumiCal is 10 cm closer to the IP relative to the ECAL.

The LumiCal consists of two cylindrical C-shaped modules surrounding the beam pipe. The inner radius is 6 cm centered on the extraction beam line with a horizontal offset of $\Delta x$ = 1.0 cm (158 cm $\times$ 0.007). The inner radius is dictated by the requirement that no detector intercepts the intense beamstrahlung pairs, which are confined within 4 cm radius by the 5 Tesla solenoid field. The longitudinal structure follows the ECAL design, consisting of 30 alternating layers of tungsten and silicon. The first 20 layers of tungsten each have thickness equivalent to 2.5 mm (or 5/7 radiation length) of pure tungsten. The last 10 layers have double this thickness, making a total depth of about 29 radiation length. The silicon sensors will be made from 6 inch wafers, and the segmentation is illustrated in Figure 2. The sensor is segmented in a $R-\phi$ geometry. A fine radial segmentation with 2.5 mm pitch is used to reach the luminosity precision goal of $10^{-3}$. The azimuthal division is 36 with each sensor covering 10 degrees. Table 1 summarizes the LumiCal parameters.

| | |
|---|---|
| z | 158 - 173 cm |
| Inner radius | 6 cm |
| Outer Radius | 20 cm |
| Fiducial | 46-86 mrad |
| Tungsten thickness | 2.5 mm (20 layers), 5.0 mm (10 layers) |
| Silicon sensor thickness | 320 $\mu$m |
| Radial division | 2.5 mm pitch |
| Azimuthal division | 36 |

Table 1: LumiCal Parameters

The BeamCal consists of two cylindrical C-shaped modules split in half horizontally to accommodate the incoming beam line. The inner radius is 2 cm centered on the extraction beam line and the outer radius is 13.5 cm. The longitudinal structure consists of 50 alternating layers of tungsten and silicon. The tungsten thickness is 2.5 mm, making a total depth of 36 radiation lengths. The silicon sensor design based on a 6 inch wafer is shown in Figure 3. The inner region less than $R < 7.5$ cm is the area where the beamstrahlung pairs would hit. The segmentation in this region is approximately 5mm $\times$ 5mm with about a half a Molière radius. This segmentation is optimized so that two-photon electron/positron can be detected in the high beamstrahlung pair background. The outer region $R > 7.5$ cm is the far LumiCal and has the same geometrical segmentation as shown in Figure 2.

Currently two electronic readout chips are being developed. The KPiX chip with 1024 channels is designed primarily for the ECAL. The chip has four hits per bunch train to be stored for each channel. The FCAL chip with 64 channels is designed to handle the 100%

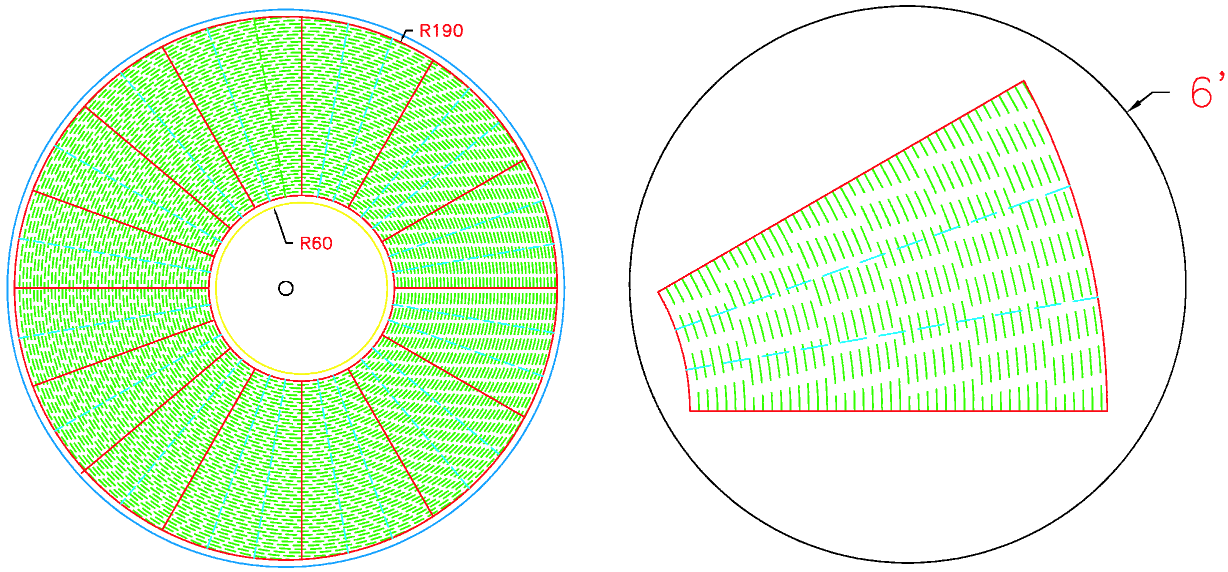


Figure 2: LumiCal sensor and segmentation.

occupancy in the BeamCal. The chip has 2820 buffer space so that a complete bunch train can be stored. Although the LumiCal occupancy is not 100%, the LumiCal region smaller than about 10 cm will have more than four hits per bunch train. Therefore, the LumiCal will use the FCAL chip in the inner region and the KPiX chip in the outer region.

## 0.4 Expected Performance

The detector performance has been studied using EGS5 [4], FLUKA [5], and GEANT4 [6] simulation packages. The ILC Nominal beam parameters at $\sqrt{s}$=500 GeV are used. Bhabha scattering is simulated using BHWIDE [7], and beamstrahlung pairs are generated using GUINEA-PIG [8]. The magnetic field map for the SiD 5 Tesla solenoid and the Anti-DID field are used.

### 0.4.1 Energy containment and energy resolution in LumiCal

One of the most important requirements for the LumiCal is the energy containment. If the energy of Bhabha events is not fully contained, some events will be classified as radiative Bhabhas and fail Bhabha event selection criteria, introducing a systematic error. Figure 4(a) shows the deposited energy (scaled by the incident energy) distribution as a function of the silicon layer from 1 GeV to 500 GeV electrons. At lower energies, the energy is mostly contained in the front 20 layers. Even at 500 GeV a significant deposition is in the front 20 layers, and the back 10 layers with double tungsten thickness accomplish the energy containment. Figure 4(b) shows the energy resolution parameter $\alpha$ in $\Delta E/E = \alpha/\sqrt{E}$ as a function of energy. The energy resolution improves at the lower energies, reaching $15\%/\sqrt{E}$ at 1 GeV, and still maintains $20\%/\sqrt{E}$ at 500 GeV.

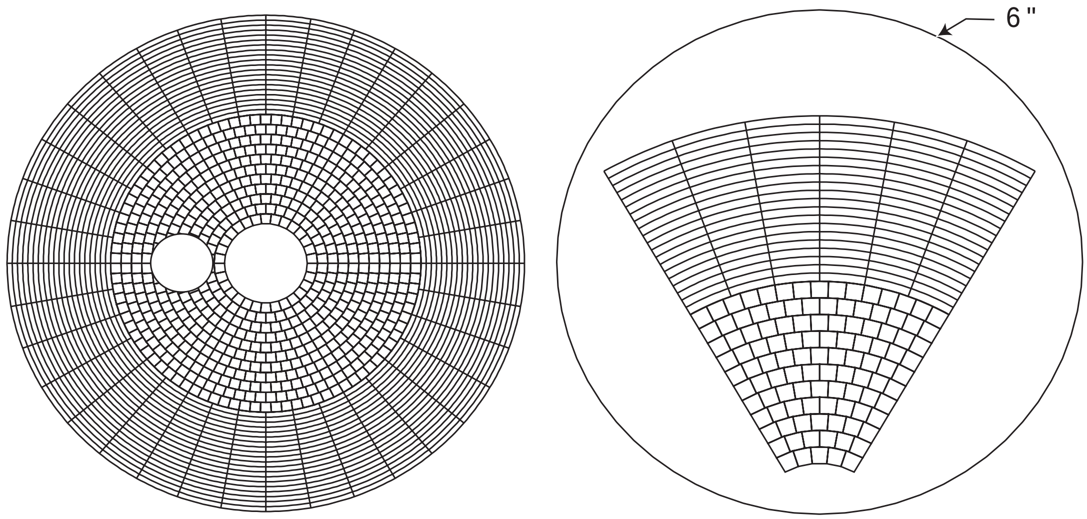


Figure 3: BeamCal sensor and segmentation.

### 0.4.2 Luminosity precision and LumiCal segmentation

The polar angle bias ($\Delta\theta$) and achievable luminosity precision have been studied as a function of sensor segmentation. Each silicon layer is segmented equally in the radial and azimuthal directions, and energy depositions in individual cells are calculated. The polar angle is reconstructed by taking a weighted average of the polar angle $\theta_i$ of individual cells with a weight $W_i$ as

$$\theta = \frac{\sum_i \theta_i W_i}{\sum_i W_i}.$$

It is well known that the electromagnetic shower development is non-linear and the weight in linear energy introduces a large bias in coordinate measurements[3] . The bias can be reduced by using so-called logarithmic weight,

$$W_i = \max\{0, \mathrm{C} + \ln(\mathrm{E_i}/\mathrm{E_{total}})\},$$

where $E_i$ is energy deposition in each cell, $E_{total}$ total energy deposition, and $C$ is a constant. The constant provides an effective energy threshold, and only cells with a large enough energy deposition are used in the polar angle reconstruction.

The LumiCal is fully simulated using 250 GeV electrons with a $1/\theta^3$ angular distribution. The reconstructed polar angle, $\theta_{rec}$ is compared with the generated one $\theta_{gen}$. The polar angle bias $\Delta\theta$ is calculated by an average value of $\theta_{rec} - \theta_{gen}$, and the angular resolution by the rms value. Table 2 shows the angular bias, angular resolution and the luminosity precision as

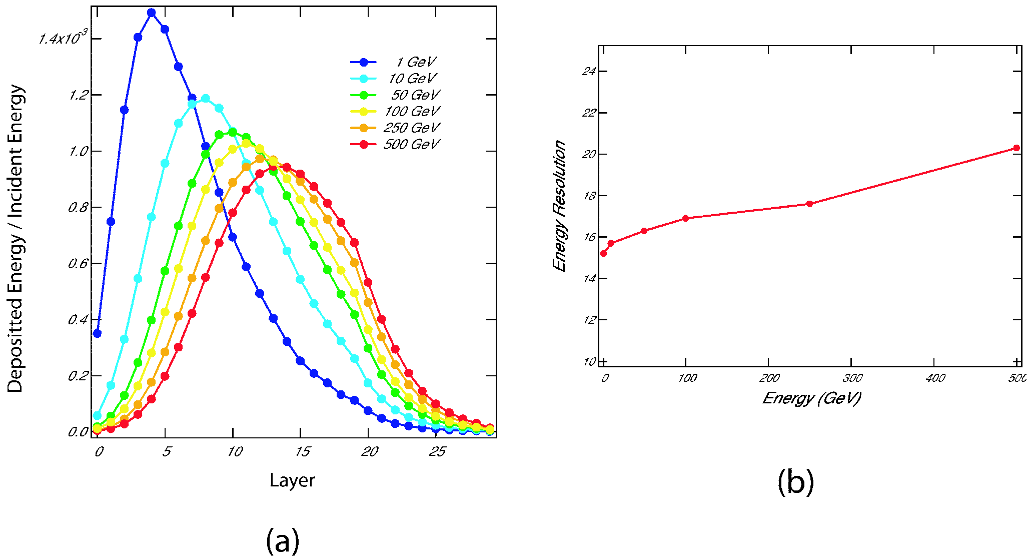


Figure 4: (a) Deposited energy in Si layers (b) Energy resolution

a function of the radial segmentation. The azimuthal segmentation is fixed to 32. The luminosity precision improves as the radial segmentation decreases, and the luminosity precision goal of $10^{-3}$ can be reached when the radial segmentation is smaller than 3 mm. The dependence on the azimuthal segmentation is studied using a fixed 2.5 mm radial segmentation. Table 3 shows the result. The luminosity precision improves as the azimuthal segmentation is decreased, but the improvement is small. Finer azimuthal segmentation would be beneficial for cluster separation.

| $\Delta r(mm)$ | $\Delta\theta(mrad)$ | $\sigma(\theta)(mrad)$ | $\Delta L/L$ |
|---|---|---|---|
| 2.0 | 0.008 | 0.042 | $3.3 \times 10^{-4}$ |
| 2.5 | 0.017 | 0.046 | $7.9 \times 10^{-4}$ |
| 3.0 | 0.023 | 0.050 | $1.0 \times 10^{-3}$ |
| 4.0 | 0.036 | 0.058 | $1.7 \times 10^{-3}$ |
| 5.0 | 0.049 | 0.069 | $2.2 \times 10^{-3}$ |

Table 2: Radial segmentation

### 0.4.3 Bhabha scattering

The LumiCal performance is studied using Bhabha events at $\sqrt{s}$=0.5 TeV. A sample of 10,000 Bhabha events is generated in the CM system by the BHWIDE event generator[7]. Each event is transferred to the laboratory system with the 14 mrad crossing angle, and then processed through the LumiCal simulation. After energy and angle reconstructions, the event is transferred back to the CM system to understand the characteristics of Bhabha events. Figure 5(a) shows the total energy distribution of the reconstructed $e^+$ and $e^-$. The

| $N\phi$ | $\Delta\theta(mrad)$ | $\sigma(\theta)(mrad)$ | $\Delta L/L$ |
|---|---|---|---|
| 16 | 0.017 | 0.046 | $7.7 \times 10^{-4}$ |
| 32 | 0.017 | 0.046 | $7.9 \times 10^{-4}$ |
| 48 | 0.017 | 0.045 | $7.6 \times 10^{-3}$ |
| 64 | 0.014 | 0.045 | $6.6 \times 10^{-3}$ |

Table 3: Azimuthal segmentation

distribution has a peak at 500 GeV as expected, and has a long tail of radiative Bhabha events. The current cluster finder can reconstruct shower above 25 GeV. Figure 5(b) shows the correlation between the reconstructed $e^-$ and $e^+$ polar angles. The 14 mrad crossing angle has been properly taken care of. The radial segmentation is visible at small angles.

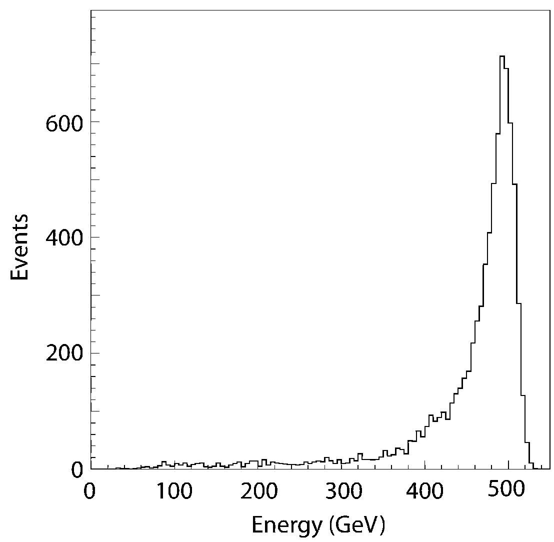


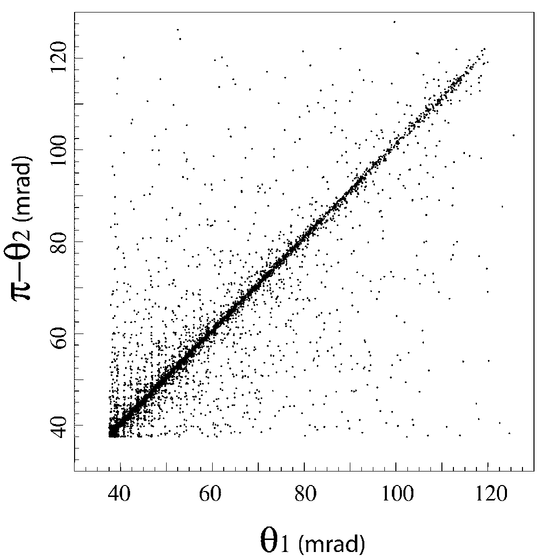


Figure 5: (a) Total energy distribution (b) Correlation of e+ and e- polar angles

### 0.4.4 High energy electron detection in BeamCal

We have studied the ability to identify and reconstruct high energy electron in the presence of beamstrahlung pair background in the BeamCal[9]. The analysis consists of three parts:

1. A lookup table which would correlate the energy and position of a shower on the BeamCal to an incident particle energy. This accounts for the $\theta$ and $\phi$ dependence of shower energy introduced by energy loss down the beampipe, and also incorporates the sampling fraction of the detector.
2. A lookup table of average beamstrahlung depositions which would be used to subtract the expected beamstrahlung energy from the shower of interest.

3. A cluster algorithm which would analyse the total signal on the BeamCal and attempt to isolate the part of the signal that is due to the high energy electron.

BeamCal signals are created by overlaying a high energy electron shower and one bunch crossing of beamstrahlung backgrounds randomly selected from the 10,000 crossings. After subtracting the average beamstrahlung energy, the cluster algolithm reconstructs the high energy electron if the subtracted energy is greater than three sigma of the beamstrahlung energy variation. As the beamstrahlung energy has a strong radial and azimuthal dependence, the recontruction efficiency is calculated as a function of the distance from the extraction beam axis at three azimuthal angles (0, 90, and 180 degrees). Figure 6 shows the reconstruction efficiency as a function of radius in the BeamCal for 50, 100, and 150 GeV electrons. The inefficiency between 30 and 50 mm at phi=180° is due to the incomming beam hole. Since the beamstrahlung background energy is the highest at phi $\approx$ 90° (and 270°), the reconstruction efficiency is lower at this angular region. Nevertheless, the efficiency to reconstruct more than 150 GeV electrons is almost 100% up to 8 mrad.

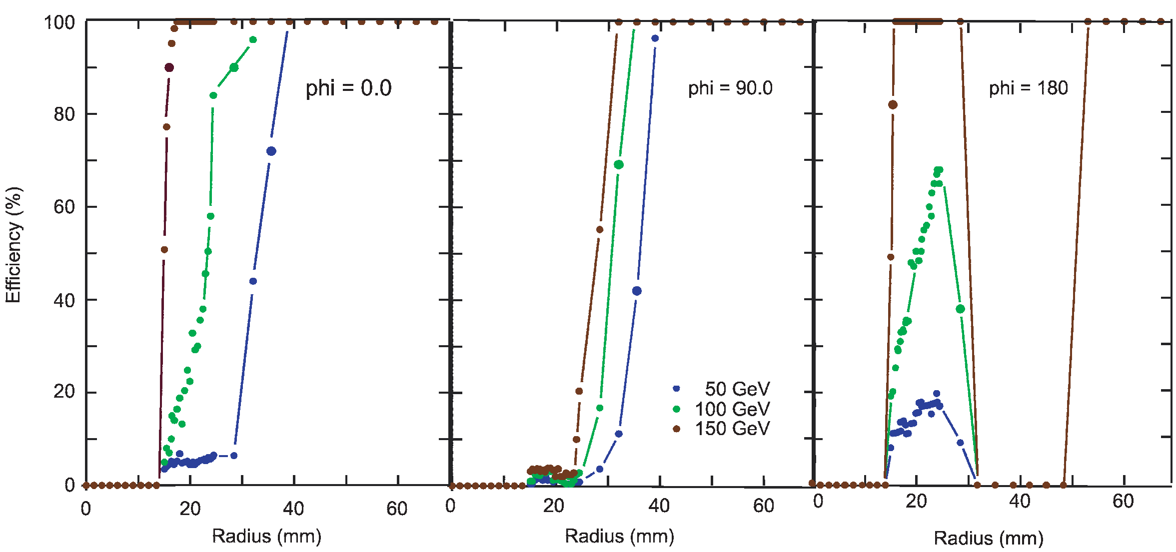


Figure 6: Efficiency to reconstruct high energy electrons at three azimuthal angles

### 0.4.5 Calorimeter hermeticity

Calorimeter hermeticity is surveyed using 250 GeV electrons. Figure 7 shows the total energy deposition in Silicon layers as a function of $\cos\theta$. The ECAL, LumiCal and BeamCal angular coverages are indicated in the figure. Five sets of simulation are made with different LumiCal Z locations. When the LumiCal is at the same Z location as the ECAL, a significant energy is lost at $\cos\theta$ ~0.993. To achieve calorimeter hermeticity, the LumiCal is moved 10 cm closer to the IP.

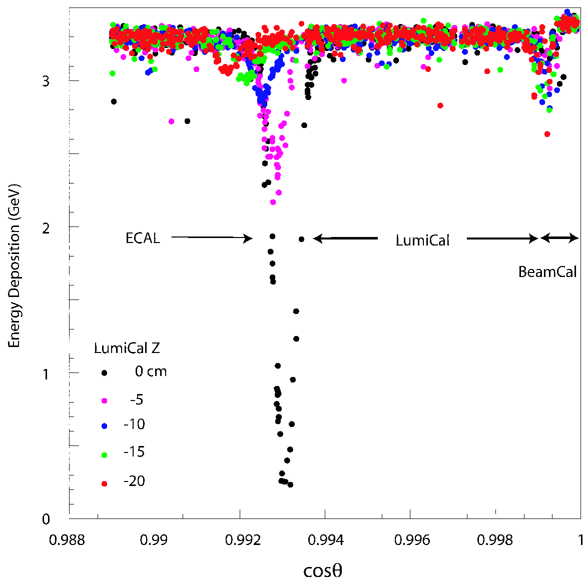


Figure 7: Energy deposition in Si layers as a functon of $\cos\theta$

### 0.4.6 Tungsten mask

When the beamstrahlung pairs hit the BeamCal, a large number of secondary photons are produced and about 35k photons per bunch crossing are back scattered. The tungsten mask is to shield the central detector from these low energy photons. Figure 8 shows the number of photons penetrating the tungsten mask as a function of the mask thickness. To eliminate the photons, a mask thicker than 6 cm is necessary. But such a thick mask takes up the space and significantly increases the weight. The mask thickness of 3 cm is chosen. Although about 1000 photons are penetrating the mask, they are low energy (∼200 KeV) and are uniformly distributed over the inner surface of Endcap HCAL.

## 0.5 R&D

The radiation level in the forward direction implies that one will need to probably specify specialized Si material. One needs to select the materials and expose them to radiation levels equivalent to what will be seen at the ILC forward region over period of 5 years. Two possible radiation hard materials are oxygenated Float Zone Si wafers and magnetic Czochralski Si wafers.

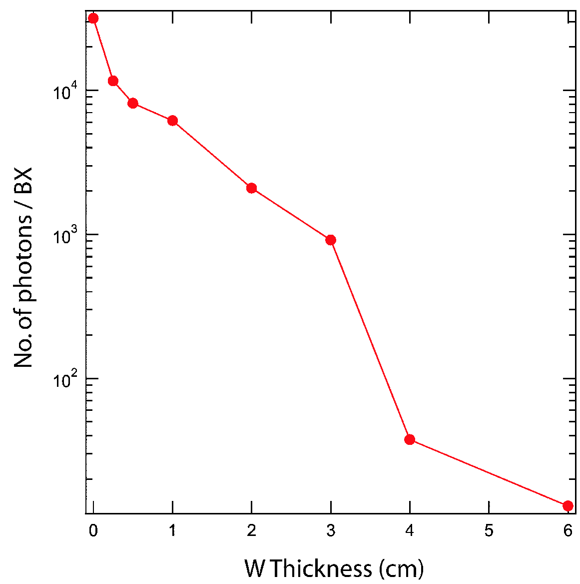


Figure 8: Number of photons penetrating the tungsten mask as a function of the mask thickness

# References


[1] "Experimental implications for a linear collider of the SUSY dark matter scenario," P. Bambade et al., arXiv:hep-ph/0406010v1, june 2004.

[2] "IR Optimization, DID and Anti-DID," A. Seryi, T. Maruyama and B. Parker, SLAC-PUB-11662, Jan. 2006.

[3] "A simple method of shower localization and identification in laterally segmented calorimeters," Nucl. Instrum. Methods A, vol. 311, 130 (1992).

[4] "The EGS5 code system," H. Hirayama, Y. Namito, A.F. Bielajew, S.J. Wilderman and W.R. Nelson, SLAC-R-730 (2005)

[5] "FLUKA: a multi-particle transport code," CERN-2005-10 (2005), INFN/TC-05/11, SLAC-R-773.

[6] "GEANT4 developments and applications," IEEE Transactions on Nuclear Science, 53, 270 (2006)

[7] "$O(\alpha)$ YFS exponentiated monte carlo for Bhabha scattering at wide angles for LEP/SLC and LEP2," Phys. Lett. B390, 298 (1997)

[8] "Study of Electromagnetic and Hadronic Background in the Interaction Region of the TESLA Collider," D. Schulte, Ph.D Thesis, Hamburg University 1996.

[9] "Electron Identification in the BeamCal of the Silicon Detector at ILC," G. Oleinik, J. Gill and U. Nauenburg, ILC-SID-TechNote-003. For details, see http://hep-www.colorado.edu/~uriel/Beamstrahl_TwoPhoton-Process/grp_results.html